RSC Advances

ROYAL SOCIETY OF CHEMISTRY

www.rsc.org/advances

RSC Advances

ARTICLE

Facile synthesis of porous CoFe$_2$O$_4$ nanosheets for lithium-ion battery anodes with enhanced rate capability and cycling stability

Xiayin Yao, Junhua Kong, Xiaosheng Tang, Dan Zhou, Chenyang Zhao, Rui Zhou and Xuehong Lu*

Porous CoFe$_2$O$_4$ nanosheets, having the thickness of 30-60 nm and lateral size of several microns with numerous penetrating pores, are synthesized via thermal decomposition of (CoFe$_2$)$_{1/3}$C$_2$O$_4$·2H$_2$O nanosheets, which are facilely prepared through a poly(vinyl alcohol)-assisted precipitation-cum-self-assembly process in an aqueous medium. The obtained porous CoFe$_2$O$_4$ nanosheets are employed as an anode in lithium-ion batteries (LIBs). The anode exhibits excellent rate capability and cycling stability. When discharging/charging at 1 A/g and 2 A/g, it can deliver discharge capacities as high as 806 mAh/g and 648 mAh/g, respectively, each for 200 cycles. This makes the porous CoFe$_2$O$_4$ nanosheets a promising candidate for anode materials in high-energy and high-power LIBs.

Introduction

Cobalt ferrite (CoFe$_2$O$_4$), a typical binary metal oxide, has been reported as a promising anode material for lithium-ion batteries (LIBs) with a high theoretical capacity of 916 mAh/g.[1,2] However, like many other transition metal oxides, CoFe$_2$O$_4$ also suffers from low rate capability resulting from its kinetic limitations as well as poor electric conductivity and poor cycling performance owing to the electrode pulverization induced by huge volume changes during repeated lithiation/delithiation processes. Generally, these problems can be partly solved by using nanostructured electrode materials. Some work on the synthesis and electrochemical properties of CoFe$_2$O$_4$ nanostructures with controllable size and shape has been reported.[3-8]

Recently, two-dimensional nanosheets have received much attention owing to their fascinating physical and chemical properties.[9] LIB electrodes composed of nanosheets could provide short pathways and high kinetics for lithium ion insertion/extraction due to their unique geometry with high surface-to-volume ratios.[10] However, up to now, there are only few published studies on the preparation of CoFe$_2$O$_4$ nanosheets, while their electrochemical properties have not been investigated.[11,12] To the best of our knowledge, there is no prior publication reporting CoFe$_2$O$_4$ nanosheets-based LIB anodes. Moreover, there are still strong demands for simple and

scalable procedures for the preparation of CoFe$_2$O$_4$ nanosheets in order to facilitate their applications as LIB anodes.

Herein, we present a simple and high-yield synthesis method for CoFe$_2$O$_4$ nanosheets through thermal decomposition of (CoFe$_2$)$_{1/3}$C$_2$O$_4$·2H$_2$O nanosheets. The obtained CoFe$_2$O$_4$ nanosheets show excellent rate capability and high-rate cycling stability when used as a LIB anode.

Experimental

All of the chemicals were analytical grade and used without further purification. The (CoFe$_2$)$_{1/3}$C$_2$O$_4$·2H$_2$O precursor was firstly prepared through a solution-based direct precipitation process using polyvinyl alcohol (PVA) as surfactant. In detail, 15g of 33.3 wt% cobalt sulfate heptahydrate and iron sulfate heptahydrate (with a molar ratio of 1:2) aqueous solution was firstly mixed with 30g of 0.3 wt% PVA aqueous solution under stirring at room temperature. Then, equivalent molar amount of 20 wt% H$_2$C$_2$O$_4$·2H$_2$O aqueous solution was introduced into the above solution. The yellow precipitates appeared immediately. After being stirred for 30 min, the precipitate was centrifugalized, washed and dried in vacuum. Finally, the solid product obtained were calcined at 600 °C with a heating rate of 2°C/min for 2h in air to obtain porous CoFe$_2$O$_4$ nanosheets.

Scanning electron microscopic (SEM) images were acquired using a JEOL-6340F field emission scanning electron microscope. Transmission electron microscopy (TEM)

experiments were performed on a JEOL 2010 transmission electron microscopy at an accelerating voltage of 200 kV. X-ray diffraction (XRD) patterns were obtained on a D8 Discover GADDS (Bruker AXS, Germany) powder diffractometer. Thermogravimetric analyses (TGA) were performed on a TGA Q500 under air atmosphere. The Brunauer-Emmett-Teller (BET) test was determined via a Micromeritics Tristar II-3020 nitrogen adsorption apparatus. Pore size distribution plot was obtained by the Barrett-Joyner-Halenda (BJH) method.

The electrochemical performances were evaluated with a standard CR2032 coin cell with lithium metal as counter electrode, Celgard 2600 as the separator, and a solution of 1.0 M $LiPF_6$ in ethylene carbonate/dimethyl carbonate (1:1 by volume) as electrolyte. The working electrode was composed of 40 wt% $CoFe_2O_4$ nanosheets, 40 wt% Super P, and 20 wt% polyvinylidene fluoride. The addition of high Super P content facilitates electron transport from the active materials to the current collector.[13] The cells were tested in the voltage range of 0.005 and 3.0 V (vs. Li^+/Li) with a Neware-CT3008 battery test system (Neware Technology Limited, Shenzhen, China). Cyclic voltammetry (CV) measurements were performed on an Autolab PGSTAT302N electrochemical workstation (Metrohm, Switzerland) at 0.1 mV/s in the voltage range of 0.005-3.0 V.

Results and discussion

The strategy for synthesis of porous $CoFe_2O_4$ nanosheets is illustrated in Fig. 1. Upon mixing, Co^{2+} and Fe^{2+} cations are immediately chelated with the OH ligands to form metal cation-PVA complex.[14,15] After oxalic acid dihydrate aqueous solution is introduced into the above precursor solution, the metal cation-PVA complex is transformed into oxalate-PVA complex, forming a yellow oxalate precipitate rapidly. Then, in the suspension, the oxalate seeds grow into nanorods with the confinement of the PVA backbone grids, and the nanorods self-assemble into nanosheets. TGA curves of PVA and oxalates nanosheets precursor are shown in Fig. 2. PVA could be totally decomposed at around 510°C. The oxalates nanosheets showed two weight losses, corresponding to the loss of crystallized water and the decomposition of the precursor, respectively. The first weight loss of 20.0% occurs at around 190°C, which is comparable to the loss of two crystallized water. The second weight loss of 36.9% occurs at around 275°C, which corresponding to the decomposition of oxalate groups as well as the conversion of anhydrous oxalate to $CoFe_2O_4$. These results indicate the obtained oxalate nanosheets consist of $(CoFe_2)_{1/3}C_2O_4 \cdot 2H_2O$. Based on the TGA analysis, the temperature for the calcination of the $(CoFe_2)_{1/3}C_2O_4 \cdot 2H_2O$ precursors to $CoFe_2O_4$ was set at 600 °C to ensure the complete decomposition of the oxalate precursor and PVA, which gives porous $CoFe_2O_4$ nanosheets.

To verify the formation of porous nanosheets, SEM studies were conducted. The morphology of the $CoFe_2O_4$ is highly dependent on the PVA aqueous solution concentrations and gradually changed from large particles to rods and nanosheets, as shown in Figure S1 in supplement material and Figure 3.
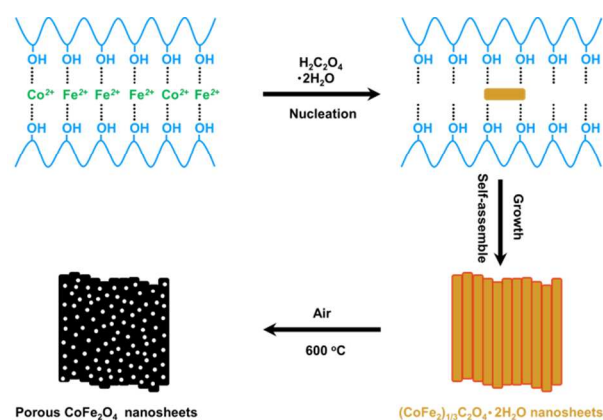
Fig. 1 Schematic illustration of the synthesis strategy for porous $CoFe_2O_4$ nanosheets.
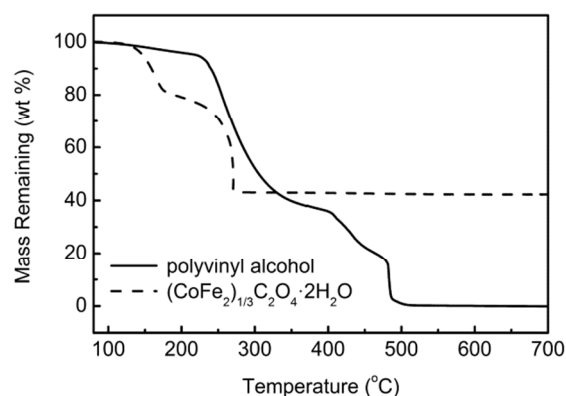
Fig. 2 TGA curves of PVA and $(CoFe_2)_{1/3}C_2O_4 \cdot 2H_2O$ contains nanosheets.

However, severe aggregations will be formed with too high PVA concentrations (e.g. 1.5 wt%, Figs. S1c and S1f). At 0.3 wt% PVA concentration, the as-synthesized $(CoFe_2)_{1/3}C_2O_4 \cdot 2H_2O$ contains nanosheets made of parallel arranged nanorods with diameters of 50-100 nm and lengths of several micrometers (Figs. 3a and 3b). After the heat-treatment in air, the oxalates are turned into $CoFe_2O_4$ porous nanosheets. Figs. 3c and 3d present SEM images of the annealed sample, confirming the porous nature of the $CoFe_2O_4$ nanosheets. The thickness of the $CoFe_2O_4$ nanosheets is decreased to 30-60 nm, which is due to the decomposition of the oxalate groups in the $(CoFe_2)_{1/3}C_2O_4 \cdot 2H_2O$ precursor. TEM studies were carried out to further reveal the structure and morphology of the porous $CoFe_2O_4$ nanosheets. It can be seen that the pores in the nanosheets are all penetrating ones with sizes of about 10-50 nm (Fig. 3e). The selected area electron diffraction (SAED) pattern of the $CoFe_2O_4$ nanosheets (the inset in Fig. 3e) shows intense reflection rings of cubic structure of $CoFe_2O_4$. The HRTEM image in Fig. 3f shows clear lattices with interplanar distance of 0.48 nm and 0.25 nm, which are consistent with the standard values for the (111) and (311) planes of the cubic structure of $CoFe_2O_4$, respectively. Fig. 3g shows the XRD patterns of the $CoFe_2O_4$ nanosheets. All the diffraction peaks
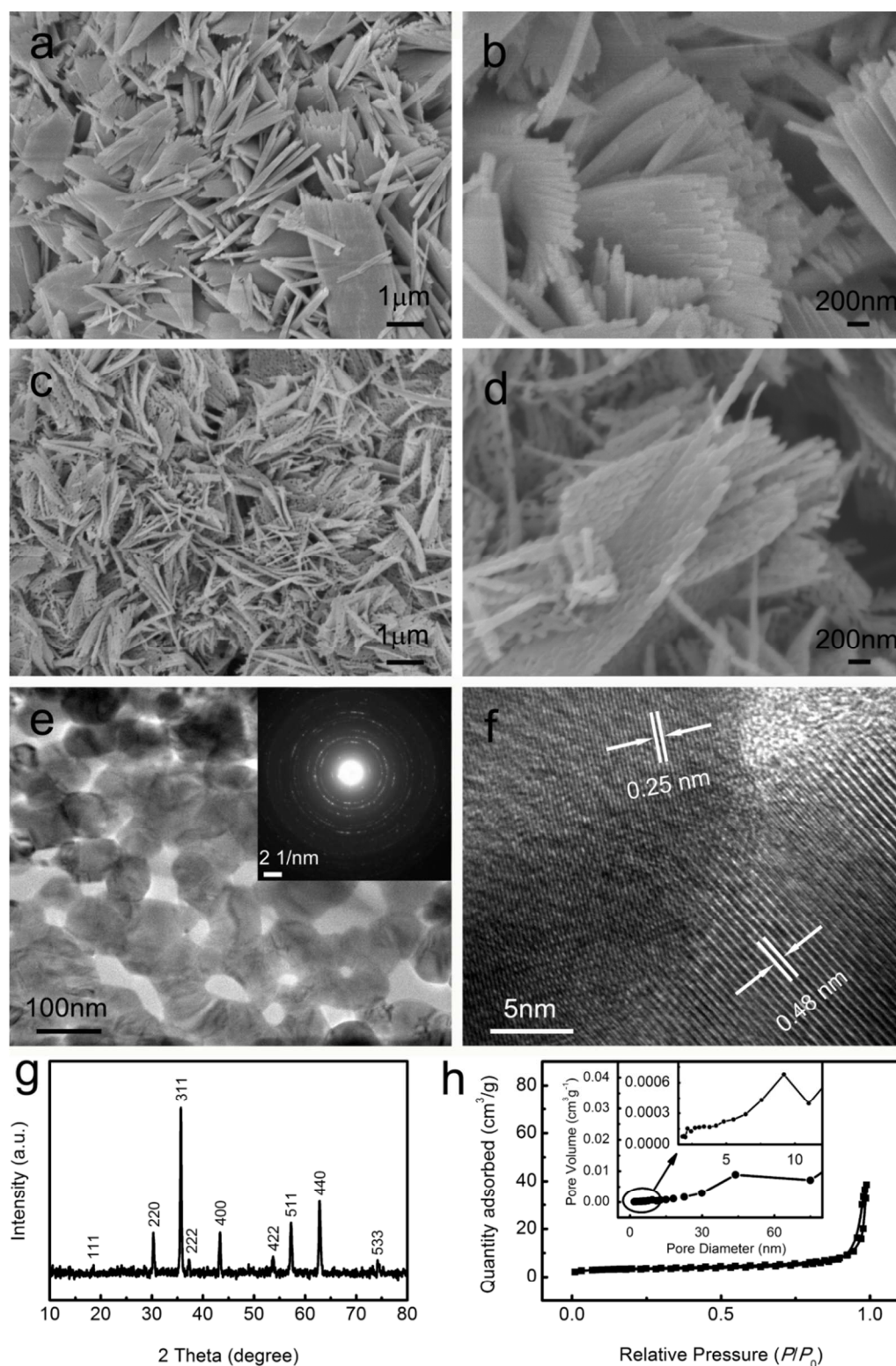
Fig. 3 SEM images of (a, b) $(CoFe_2)_{1/3}C_2O_4 \cdot 2H_2O$ and (c, d) $CoFe_2O_4$ nanosheets. (e) TEM and (f) HRTEM images of an individual $CoFe_2O_4$ nanosheet; the inset in (e) is the corresponding SAED pattern. (g) XRD pattern and (h) nitrogen adsorption-desorption isotherm of the $CoFe_2O_4$ nanosheets; the insets in (g) are the corresponding BJH pore size distribution curves.

can be indexed to the cubic structure of spinel $CoFe_2O_4$ (JCPDS: No. 22-1086), which support the SAED and HRTEM results.

The porosity of the $CoFe_2O_4$ nanosheets was further characterized by BET measurements. The BET results are shown in Fig. 3h and the insets are the corresponding BJH pore
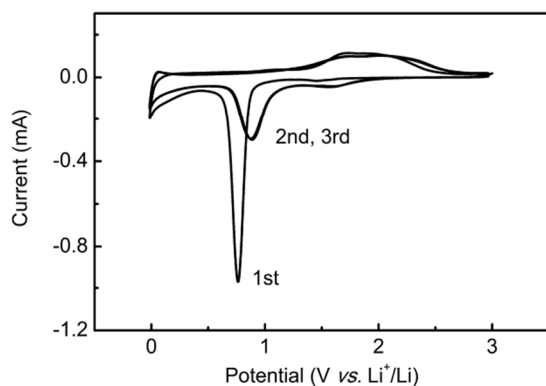
Fig. 4 Cyclic voltammogram of the CoFe$_2$O$_4$ nanosheets.

contact area between the electrode and electrolyte, providing more sites for lithium-ion insertion/extraction. Moreover, the pores may act as buffer spaces to alleviate the volume expansion during the lithiation/delithiation processes, improving cycling stability of the electrode.[14]

The electrochemical properties of the porous CoFe$_2$O$_4$ nanosheets were evaluated with a standard CR2032 coin cell. Fig. 4 shows the CV curves of the cell to elucidate the electrochemical process of the CoFe$_2$O$_4$ electrode. Obviously, there is a large difference between the curves for the first and subsequent cycles, indicating their different reaction mechanisms. In the first cycle, there is a sharp peak at around 0.75V in the cathodic process, which can be ascribed to the reduction of Fe^{3+} and Co^{2+} to their metallic states and the formation of Li$_2$O, as well as the decomposition of organic electrolyte to form a solid electrolyte interphase (SEI) layer.[3] Meanwhile, a broad peak appears at about 1.8 V in the anodic process, which corresponds to the multi-step oxidation of metallic Fe and Co to Fe^{3+} and Co^{2+}, respectively. In the subsequent cycles, the cathodic peaks shift to higher potentials compared with the initial one, further confirming the multi-step electrochemical reactions.[5] A significant decrease of the areas enclosed by the CV curves from the first to the second cycle implies an irreversible capacity loss in the initial lithiation/delithiation process. However, the peak currents and the enclosed areas are almost constant from the second cycle onwards, indicating the good electrochemical reversibility of the porous CoFe$_2$O$_4$ nanosheets electrode.

size distribution curves. It can be seen that the dominant pore sizes deduced using the BJH method are about 43 nm for the CoFe$_2$O$_4$ nanosheets, which is consistent with the SEM and TEM observations (Figures 3d and 3e). The pore size distribution curve also shows that there are possibly some smaller pores with size of about 9 nm. Indeed, the presence of small pores of less than 10 nm is confirmed by the high-magnification SEM image of a CoFe$_2$O$_4$ nanosheet (Figure S2 in supplement material). The appearance of pores with different sizes is probably caused by the release of CO$_2$ during the decomposition of (CoFe$_2$)$_{1/3}$C$_2$O$_4\cdot$2H$_2$O as well as the interspaces between some stacked CoFe$_2$O$_4$ nanosheets. The BJH adsorption cumulative volume of pores is 0.057 cm^3/g. The specific surface area estimated from the BET results is 12.13 m^2/g. It is worth noting that the porous morphology would benefit the transport of lithium ions owing to the large

Figs. 5a and 5b present the charge/discharge profiles, cycling behavior and coulombic efficiency of the porous CoFe$_2$O$_4$ nanosheets electrode in the first 30 cycles at 50 mA/g. It can be seen that the electrode exhibits a discharge potential
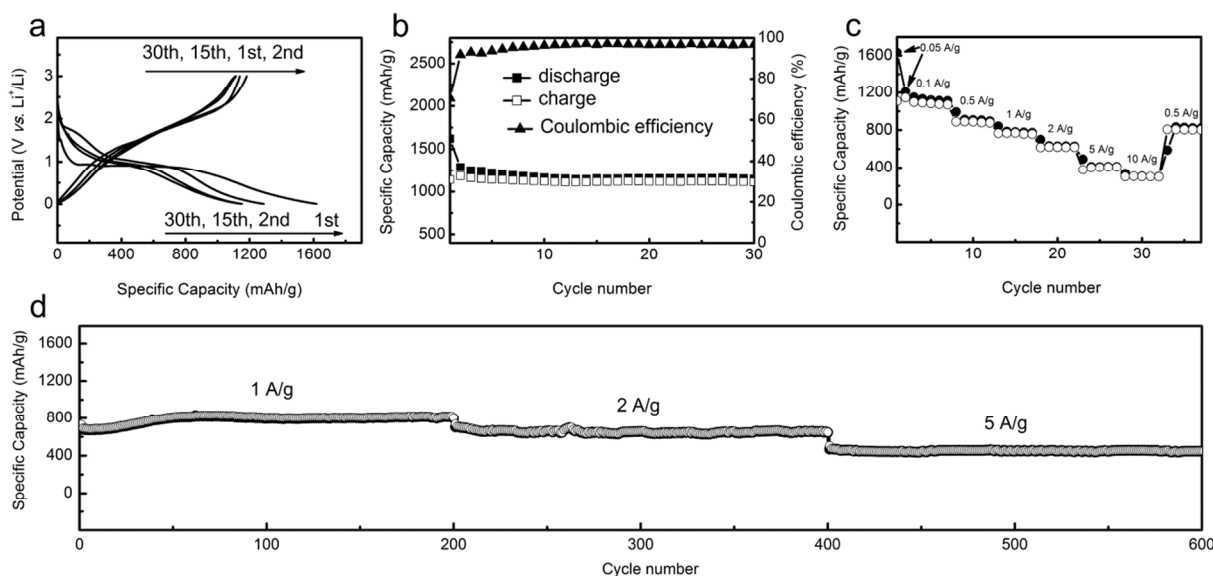
Fig. 5 Electrochemical properties of the porous CoFe$_2$O$_4$ nanosheets as an anode in coin cell: (a) galvanostatic charge/discharge profiles, (b) cycling performance and Coulombic efficiency at 50 mA/g, (c) capacities at different current densities and (d) cycling performance at different current densities.
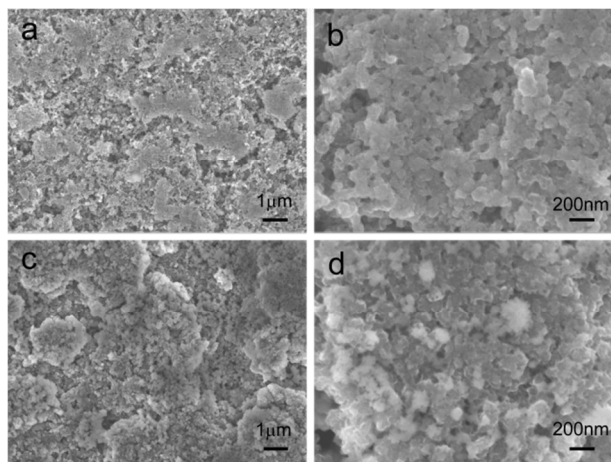
Fig. 6 SEM images of porous CoFe$_2$O$_4$ nanosheets electrodes after (a, b) 30 cycles at 50 mA/g and (c, d) after 600 cycles from 1, through 2, to 5 A/g.

plateau at around 0.85 V, and delivers an initial discharge capacity of 1619 mAh/g and charge capacity of 1139 mAh/g, with a Coulombic efficiency of 70.4 %. A large capacity loss between the 1st and 2nd cycles can be observed, which is due to the formation of a solid electrolyte interphase layer on the electrode surface during the 1st discharge process.[16] These are consistent with the aforementioned CV results. Nevertheless, the charge and discharge capacities stabilize during the following cycles, and the Coulombic efficiency is increased to above 90%, suggesting excellent capacity retention of the porous CoFe$_2$O$_4$ nanosheets electrode. Up to the 30th cycle, the discharge and charge capacities maintain at 1147 mAh/g and 1111 mAh/g, respectively, which are higher than those of other CoFe$_2$O$_4$-based anodes reported in literatures.[5,7,8]

Fig. 5c shows the rate capabilities of the porous CoFe$_2$O$_4$ nanosheets anode at various current densities ranging from 0.1 to 10 A/g. The anode delivers discharge capacities of 1112, 896, 773, 628, 413, 303 mAh/g at 0.1, 0.5, 1.0, 2.0, 5.0, 10 A/g, respectively, demonstrating its excellent rate capability. Furthermore, when the current density was reset to 0.5 A/g, the capacity could recover to 823 mAh/g. The cyclic performance was also investigated at high rates (Fig. 5d). The reversible discharge capacities can be maintained at 806, 648, 448 mAh/g at 1.0, 2.0 and 5.0 A/g, respectively, each for 200 cycles. The slight increase in capacity in the first 100 cycles may be ascribed to an activation process owing to the improved contact between the active material and electrolyte upon charge and discharge.[17] The excellent capacity performance and long-term cycling stability of the porous CoFe$_2$O$_4$ nanosheets electrode at high current densities can be attributed to the short pathways and high kinetics for lithium ion insertion/extraction provided by the two-dimensional nanostructure as well as the numerous penetrating pores in the nanosheets that offer more reactive sites and alleviate the volume expansion during the lithiation/delithiation processes.

To further gain an insight into the superior rate capability and cycling stability, the microstructures of the electrode material after 30 cycles at 50 mA/g as well as after long-term cycling at high rates were characterized by SEM. The results are shown in Fig. 6. It can be seen that the porous nanosheet morphology of CoFe$_2$O$_4$ can be retained after cycling even at high current densities. After 30 cycles at 50 mA/g, the porous morphology can be clearly observed (Figs. 6a and 6b). After 600 cycles from 1, through 2, to 5 A/g (as described in Fig. 5), although there seems to be less large pores, small pores can still be clearly observed (Figs. 6c and 6d). The relatively stable porous morphology of the CoFe$_2$O$_4$ nanosheets during cycling provides evidence for the superior rate capability and cycling stability of the CoFe$_2$O$_4$ nanosheet-based electrode.

Conclusions

We have presented a facile and effective route for synthesizing porous CoFe$_2$O$_4$ nanosheets from decomposition of (CoFe$_2$)$_{1/3}$C$_2$O$_4$·2H$_2$O, and it can be employed for large-scale production. The as-synthesized CoFe$_2$O$_4$ nanosheets, with the thickness of 30-60 nm and lateral size of several microns, were investigated as an anode in LIBs. The anode shows excellent rate capacity and cycling stability; it is able to maintain stable reversible discharge specific capacities of 806 mAh/g and 648 mAh/g at 1.0 A/g and 2.0 A/g, respectively, each for 200 cycles. The high lithium storage capacity and excellent rate capability as well as high-rate cycling stability, in combination with the simple and scalable preparation procedures, make the CoFe$_2$O$_4$ porous nanosheets a promising candidate for anode materials in next generation high-energy and high-power LIBs.

Notes and references

School of Materials Science and Engineering, Nanyang Technological University, 50 Nanyang Avenue, 639798, Singapore
E-mail: ASXHLu@ntu.edu.sg (Prof. X. Lu)

1   Y. Q. Chu, Z. W. Fu and Q. Z. Qin, *Electrochim. Acta*, 2004, **49**, 4915-4921.

2   Y. N. NuLi and Q. Z. Qin, *J. Power Sources*, 2005, **142**, 292-297.

3   Y. Wang, D. W. Su, A. Ung, J. H. Ahn and G. X. Wang, *Nanotechnology*, 2012, **23**, 055402.

4   M. X. Li, Y. X. Yin, C. J. Li, F. Z. Zhang, L. J. Wan, S. L. Xu and D. G. Evans, *Chem. Commun.*, 2012, **48**, 410-412.

5   Y. Wang, J. Park, B. Sun, H. Ahn and G. Wang, *Chem. Asian J.*, 2012, **7**, 1940-1946.

6   Z. L. Zhang, Y. H. Wang, M. J. Zhang, Q. Q. Tan, X. Lv, Z. Y. Zhong and F. B. Su, *J. Mater. Chem. A*, 2013, **1**, 7444-7450.

7   S. Y. Liu, J. Xie, C. C. Fang, G. S. Cao, T. J. Zhu and X. B. Zhao, *J. Mater. Chem.*, 2012, **22**, 19738-19743.

8   H. Xia, D. D. Zhu, Y. S. Fu and X. Wang, *Electrochim. Acta*, 2012, **83**, 166-174.

9   M. Chhowalla, H. S. Shin, G. Eda, L. J. Li, K. P. Loh and H. Zhang, *Nature Chem.*, 2013, **5**, 263-275.

10 D. Rangappa, K. D. Murukanahally, T. Tomai, A. Unemoto and I. Honma, *Nano Lett.*, 2012, **12**, 1146-1151.

RSC Advances Accepted Manuscript

11 H. Yang, Y. C. Mao, M. Y. Li, P. Liu and Y. X. Tong, *New J. Chem.*, 2013, **37**, 2965-2968.

12 M. Y. Li, Y. C. Mao, H. Yang, W. Li, C. S. Wang, P. Liu and Y. X. Tong, *New J. Chem.*, 2013, **37**, 3116-3120.

13 B. Kang and G. Ceder, *Nature*, 2009, **458**, 190-193.

14 X. Y. Yao, C. L. Tang, G. X. Yuan, P. Cui, X. X. Xu and Z. P. Liu, *Electrochem. Commun.*, 2011, **13**, 1439-1442.

15 X. Y. Yao, X. Xin, Y. M. Zhang, J. Wang, Z. P. Liu and X. X. Xu, *J. Alloy. Compd.*, 2012, **521**, 95-100.

16 J. W. Xiao, G. L. Xu, S. G. Sun and S. H. Yang, *Part. Part. Syst. Char.*, 2013, **30**, 893-904.

17 L. Qie, W. M. Chen, Z. H. Wang, Q. G. Shao, X. Li, L. X. Yuan, X. L. Hu, W. X. Zhang and Y. H. Huang, *Adv. Mater.*, 2012, **24**, 2047-2050.

Graphical abstract

Facile synthesis of porous CoFe$_2$O$_4$ nanosheets for lithium-ion battery anodes with enhanced rate capability and cycling stability

Xiayin Yao, Junhua Kong, Xiaosheng Tang, Dan Zhou, Chenyang Zhao, Rui Zhou and Xuehong Lu*

School of Materials Science and Engineering, Nanyang Technological University, 50 Nanyang Avenue, 639798, Singapore
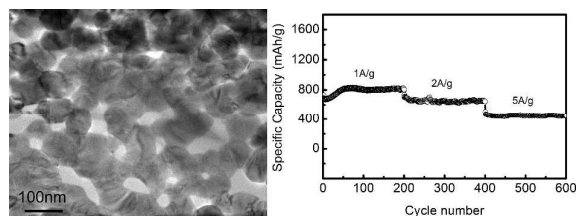
Porous CoFe$_2$O$_4$ nanosheets are prepared via a low-cost and scalable process and demonstrated as high-performance anode materials for lithium-ion batteries.